SOLUTION-PROCESSED LOW-VOLTAGE ORGANIC FIELD-EFFECT TRANSISTORS BASED ON ANTHRADITHIOPHENE MOLECULAR SOLIDS

by

Wenmin Guo

A thesis submitted to Johns Hopkins University in conformity with the requirements for the degree of Master of Science in Engineering

Baltimore, Maryland

May, 2014

ABSTRACT

Solution-processed low-voltage organic field-effect transistors (OFETs) have attracted much attention due to their possible application in the fabrication of devices with large area, light weight, low cost and flexibility. This project includes the design and optimization of solution-processed low-voltage organic phototransistors (OPTs) and biosensors which respond to bovine serum albumin (BSA).

The OPT device was based on triethylgermylethynyl-substituted anthradithiophene (diF-TEG ADT). Two kinds of dielectric materials were used: 80-nm-thick potassium alumina (PA) and 300-nm-thick thermally grown SiO_2. To investigate application in a moist environment, the performance at different relative humidities (R.H.'s) was characterized. Results showed that the device was very stable in high humidity, and exhibited good performance even up to 85% R.H. A major change in drain current (I_{DS}) was observed when connecting or disconnecting the gate electrode to the device in the dark once the photocurrent was generated. This feature may motivate the application of diF-TEG ADT-based phototransistors as multistage photo-controlled memory devices.

For the biosensor device, a sensitive (10 ng/mL) sensor platform for bovine serum albumin (BSA) detection using small molecule-polymer blend transistor was developed. Triethylsilylethynyl-substituted anthradithiophene (diF-TES ADT) was

used as the small molecule semiconductor. Blending poly(methyl methacrylate) (PMMA) with diF-TES ADT improved the environmental and electrical stability since they are reported to form a vertically phase-separated structure. The high stability in 0.05 PBS solution and small leakage current also contributed to the application of this device as a biosensor. Moreover, the solution rheology of polymers makes it easier to print them on large flexible substrates.

Reader (Thesis advisor): Professor Howard E. Katz

ACKNOWLEDGEMENT

First, I would like to express my gratitude to my supervisor, Professor Howard Katz. Without his kind permission, I couldn't have had the chance to work in this amazing lab. During my graduate study at Johns Hopkins University, he has always been encouraging me. He provides us a great research environment. With his encouragement, I come into contact with many new ideas from which I've learned a lot. I appreciate his vast knowledge and skill in our research field.

Gratitude is also expressed to Dr. Weiguo Huang, who taught me device building hand by hand and gave me many helpful suggestions when I met with bottlenecks. I would not have been able to finish my master's research without the aid and support of Weiguo. I'd also like to thank Yu Liu, Srinivas Kola, Jasmine Sinha and all the other Katz group members. I would like to thank Jeanine Majewski, who is a staff member in the Materials Science and Engineering Department. She provided a lot of assistance during my student life at Johns Hopkins University. We thank Professor John Anthony of the University of Kentucky for graciously supplying the anthradithiophene semiconductors.

Finally, I'd like to thank my parents and my friends for the support they provided me through my life. My mum Zheng Guo and my dad Changan Guo are always on my side. Without their encourage, I cannot adjust to the life in a foreign country in a short time and devote all my energies to the experiments. I'd also like to thank my boyfriend Huan Yue and my roommates Ziyao Wang, Wei Zhuang and Yuan Gao. They always keep me company when I am lonely. I love you all!

TABLE OF CONTENTS

LIST OF FIGURES

Chapter 1

Organic Phototransistors Based on diF-TEG ADT Molecular Solid

1.1 Introduction

Organic field-effect transistors (OFETs) have attracted much attention due to their possible application in the fabrication of devices with large area, light weight, flexibility, and low cost. The performance of OFETs depends on various parameters, the main ones being charge carrier mobility (μ) and threshold voltage (V_T). In the last two decades, progress in organic semiconductors research has led especially to great increases in carrier mobility [1, 2, 3].

An interesting alternative application of OFET technology is the organic phototransistor (OPT). Its current can be modulated by both light and electric fields. Charge transport phenomena, the ability to generate photo-induced charge, and mechanical flexibility are helpful for the application of OFETs to optoelectronic devices[4]. In addition to charge carrier mobility and threshold voltage, the key parameters for evaluating the performance of OPTs are photocurrent/dark-current ratio (P) and photoresponsivity (R),

$$P = \frac{I_{DS,illu} - I_{DS,dark}}{I_{DS,dark}} \tag{1.1}$$

$$R = \frac{I_{ph}}{P_{ill}} = \frac{I_{DS,illu} - I_{DS,dark}}{P_{in}A} \tag{1.2}$$

where $I_{DS,illu}$ and $I_{DS,dark}$ are the drain current under illumination and in the dark, A is the area of the active region of the transistor under illumination, and P_{in} is the illumination intensity. High phototcurrent/dark-current ratio and photoresponsivity are desired for organic phototransistors. OPTs based on crystalline anthracene microplates[5] exhibited a relatively high phtotocurrent/dark-current ratio ($> 1.4 \times 10^5$, $\mathrm{I} = 1.4\ \mu\mathrm{W/cm^2}$) and photoresponsivity ($1.1 \times 10^4\ \mathrm{A/W}$). Kim et al.[6] fabricated OPTs based on crystalline microribbons with a high photocurrent/dark-current ratio (1.2×10^6, $\mathrm{I} = 5.6\ \mu\mathrm{W/cm^2}$). A large photoresponsivity of $1.2 \times 10^4\ \mathrm{A/W}$ ($30\ \mu\mathrm{W/cm^2}$) was obtained from OPTs based on 6-methyl-anthra[2,3-b]benzo[d]thiophene crystalline microribbons[7]. To date, the best photoresponsivity for OPTs was $4.08 \pm 1.65 \times 10^5\ \mathrm{A/W}$ using single fibers from perylenebis (dicarboximide)s (PDI)[8].

Linear acenes have attracted much attention in electrical applications due to their carrier mobility and excellent intermolecular π-interactions. Pentacene is one of the original p-type organic semiconductors and is commercially available[9]. However, the costs associated with vacuum processes needed for pentacene-based thin films makes the application of pentacene as OPTs more expensive. In addition, the limited chemical stability and oxidation rates in air make pentacene less reliable. Functionalized pentacene organic semiconductors were reported to show a persistent photoconductivity effect[10], but this effect has yet to be observed in functionalized heterocyclic analogs. Difluoro-triethylgermylethynyl-substituted anthradithiophene

(diF-TEG ADT)[1] (Figure 1.1) is a new member of the linear acene family, kinetically protected and solubilized with triethylgermylethynyl groups in positions 6 and 13 of the ADT[11]. Moreover, the addition of two fluorine substituents not only enhances the stability of the organic material but also emphasized the two-dimensional π-stacked arrangement. Therefore, we introduced diF-TEG ADT-based materials for fabrication of crystalline thin films due to their highly solubility and high degree of intermolecular interactions.

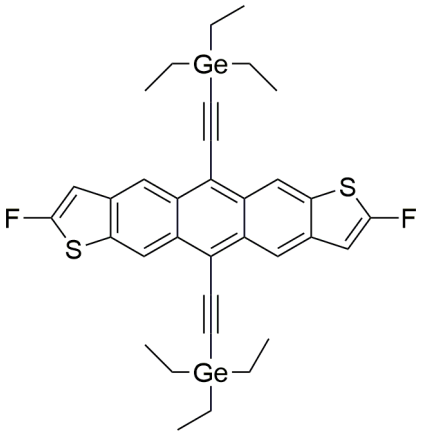

Figure 1.1 The molecule structure of diF-TEG ADT

Low power consumption is of great importance for the application of optoelectronic devices, especially for phototransistor devices. The majority of reported organic devices operate at high voltages, typically from 10 to 100V. However, most targeted applications of OPTs, such as portable and battery-powered photosensors or digital imagers preferably operate at lower voltages[12]. Low-voltage operated and low-power ambipolar OPTs based on pentacene/$PC_{61}BM$ heterostructure had been investigated and a self-assembled monolayer (octadecylphosphonic acid) was used as the gate

dielectric. These transistors could operate below 3V or -3V[12]. However, the fabrication of pentacene again needs high vacuum deposition. A 7, 7, 8, 8-tetracyanoquinodimethane (TCNQ)-based low-voltage OPT had also been reported[13]. It exhibited stable n-type characteristics with a photosensitivity >1 mA/W at an optical power of $5.98\ \mathrm{mW/cm^2}$.

To examine the stability of devices in moisture, we investigated the performance of diF-TEG ADT devices at various humidities. For portable and battery-powered photosensors and biosensors, the ability to withstand high humidity could be crucial. However, very few relevant studies have been published. In addition, the significant change in I_{DS} when disconnecting the gate probe motivated a new application of this device: four-stage photo-controlled memory.

In this project, we describe a low-voltage solution-processed OPT which can operate at -3V, a voltage compatible with high humidity. The illumination intensity we used is $112\ \mu\mathrm{W/cm^2}$ and the maximum photosensitivity reached up to $1.35\ \mathrm{A/W}$ for a PA-dielectric device under $V_G = -3\,V$. Under illumination, the drain current was increased nearly 1.45 μA at $V_D = -3\,V$ ($V_G = -2.1\,V$).

1.2 Experimental Section

1.2.1 Device fabrication

The diF-TEG ADT was synthesized as previously reported by Anthony[1]. The OPTs were fabricated with a bottom-gate, top-contact configuration. A heavily doped n-type Si wafer was used as a gate electrode. The wafer was cleaned with ultrasonication in piranha solution **(DANGER! Highly corrosive to skin!)**, acetone and isopropanol, and dried by forced nitrogen gas. Two kinds of dielectric layers were investigated: 80-nm-thick potassium alumina (PA) and 300-nm-thick thermally grown SiO_2. The semiconductor thin film was prepared by first drop-casting 0.4 mg/mL diF-TEG ADT solution in chlorobenzene onto the dielectric layer, followed by crystalizing in vacuum oven at 60℃ for 3h. Then the gold source and drain electrodes (50nm) were thermally evaporated through an interdigitated mask (as shown in Figure 1.2, channel width/length (24000μm/400μm)) at 0.3 $\text{Å}\,s^{-1}$. The deposition chamber pressure was $<5\times10^{-6}$ Torr.

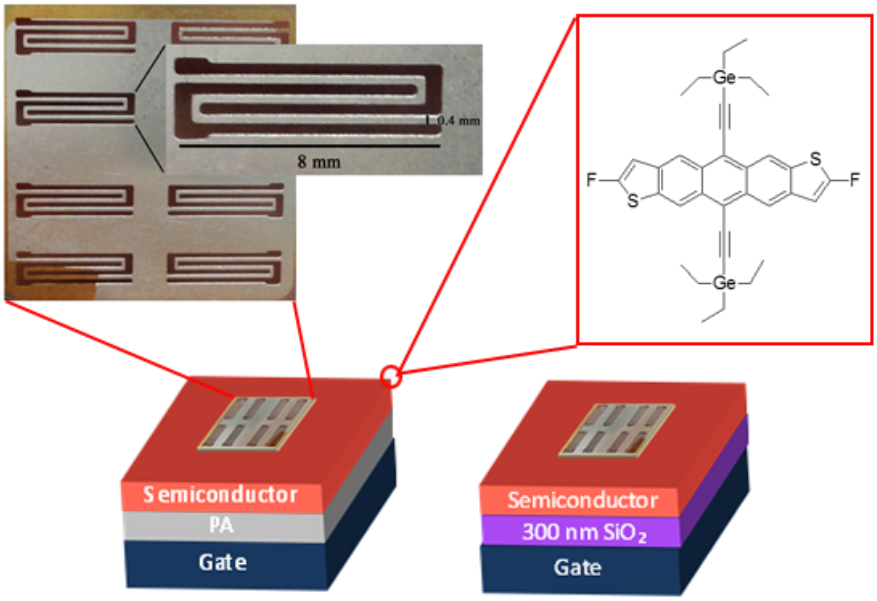

Figure 1.2 Device architecture of OPTs with the interdigitated electrode mask used for fabricating device

1.2.2 Preparation of the PA dielectric layer

The PA dielectric layer was prepared by the sol-gel spin-coating method[14]. The ion-incorporated alumina precursor solution (0.5 M) was obtained by dissolving aluminum nitrate nonahydrate (Sigma Aldrich) and potassium metabisulfite (Alfa Aesar) (11:1 molar ratio) into 2-methoxyethanol solvent. Then 0.5 M acetylacetone was added into the solution as stabilizer. The mixed solution was then stirred at room temperature for 3 h. As-prepared precursor solution was kept for 24 h to promote hydrolysis and filtered through a 0.45 μm PTFE filter. The alumina precursor was spin-coated twice on the device at 3000 rpm for 30s. It was annealed at 200 ℃ for 30 min after the first spin-coating and finally annealed at 500 ℃ for 1 h after the second spin-coating.

1.2.3 Electrical and photoresponse characterization of the devices

All the OPTs were characterized using an Agilent 4155C semiconductor analyzer. During phototransistor performance characterization, $V_G = V_D = -3\,V$ (for PA-dielectric device) or $V_G = V_D = -20\,V$ (for SiO_2-dielectric device) were used. UV-Vis absorption measurements on diF-TEG ADT solution in chloroform and films drop-cast (chlorobenzene solution) on quartz were carried out using a Shimadzu UV-3100 spectrophotometer. To study the photoresponse, devices were characterized

under illumination using a UV light (λ = 365nm, illumination intensity = 112 $\mu W/cm^2$). The illumination intensity was measured using an OPHIR meter. To obtain reproducible results under illumination, the devices were tested repeatedly in the dark until the electrical performance of the devices stabilized. To test the performance in moisture, the device and the semiconductor analyzer were placed in a dark box. A ULTRA-NEB100 (DEVILBISS) moisture generator was used to produce the moist environment and the humidity was displayed by a HS-2000 humidity meter.

1.3 Results and Discussion

1.3.1 Current voltage characteristics of OPTs

Figures 1.3 and 1.4 summarize the electronic characteristics for diF-TEG ADT-based OPTs. The transfer curves of devices with two kinds of dielectric layers are given in Figure 1.3. The output curves of PA-dielectric devices in the dark (Figure 1.4 (a)) and under illumination (Figure 1.4 (b)) demonstrate that the photo-induced charges made it easier for the FETs to turn on. Although the "turn on" phenomenon for SiO_2-dielectric device was not as obvious as for the PA-dielectric device (Figure 1.4 (c) and (d)), the ratio of $I_{DS,illu}/I_{DS,dark}$ reached 2.0×10^2 at $V_D = -20\,V, V_G = 0V$.

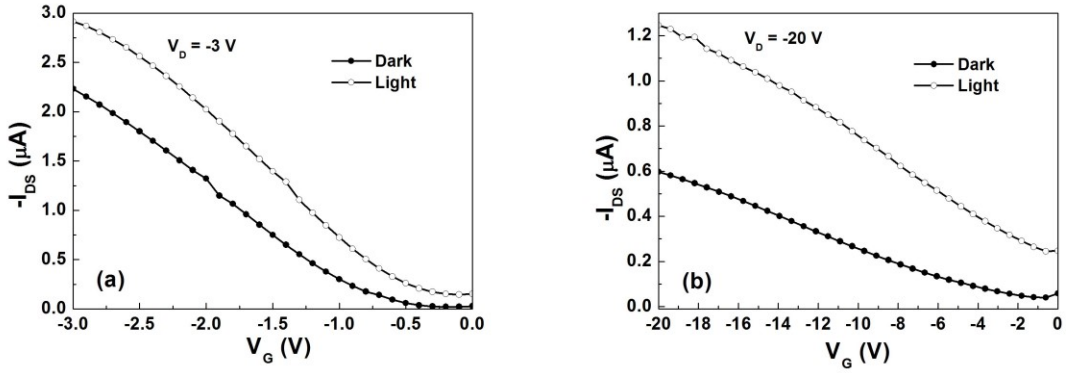

Figure 1.3 The transfer characteristics of OPTs with (a) PA dielectric layer and (b) SiO_2 dielectric layer in the dark and under illumination

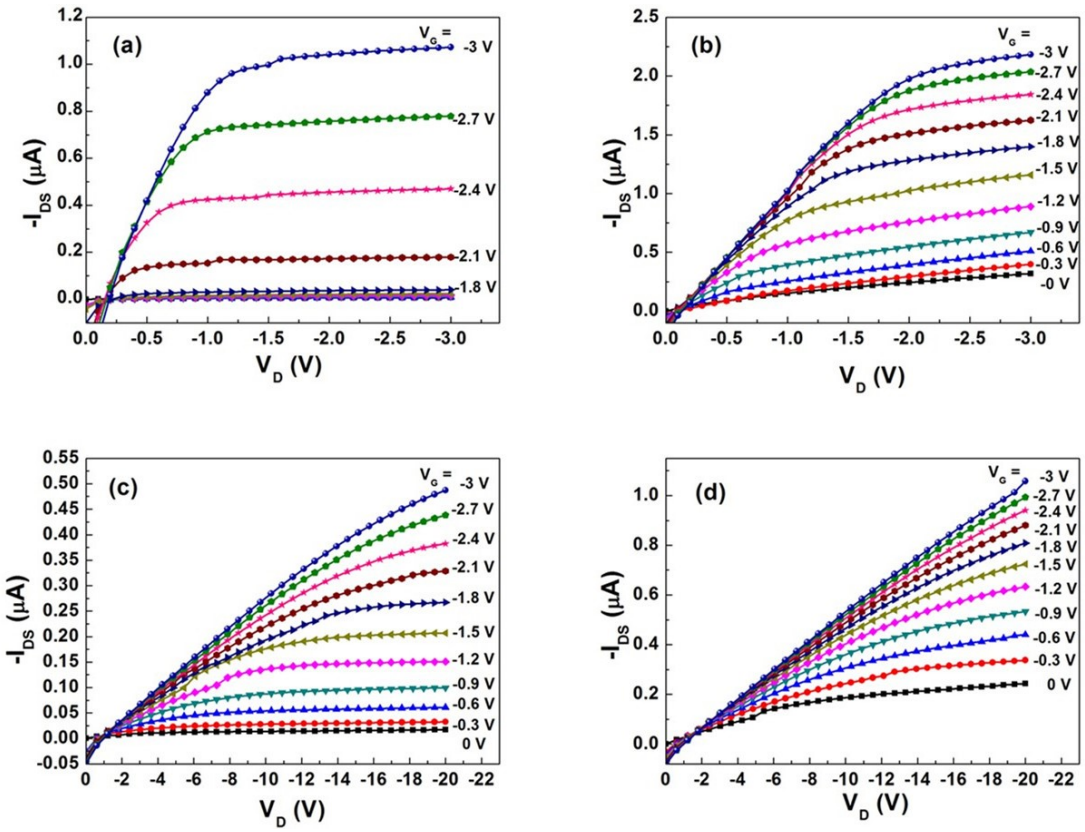

Figure 1.4 Output curves of OPTs with PA dielectric layer (a) in the dark and (b) under illumination. Output curves of OPTs with SiO_2 dielectric layer (c) in the dark and (d) under illumination

The UV-Vis absorption spectra of solution (i) and film (ii) are shown in Figure 1.5. The absorption spectrum of the film was broadened and red-shifted, a sign of strong intermolecular interactions. The absorption peak in the ultra-violet region was at ~300 nm for the solution sample. Based on the red-shift in the visible region, the peak wavelength for the film in the ultra-violet region should be larger than 300 nm. In this work, 365 nm-wavelength UV light source was used in measuring the photoresponse of diF-TEG ADT-based OPTs. Photons absorbed by the diF-TEG ADT create excitons which will dissociate into electron-hole pairs. The holes that do not undergo recombination should contribute to the photocurrent. Optimized performance would be obtained if the wavelength of the light source matched the peak wavelength of diF-TEG ADT UV-Vis spectrum[15].

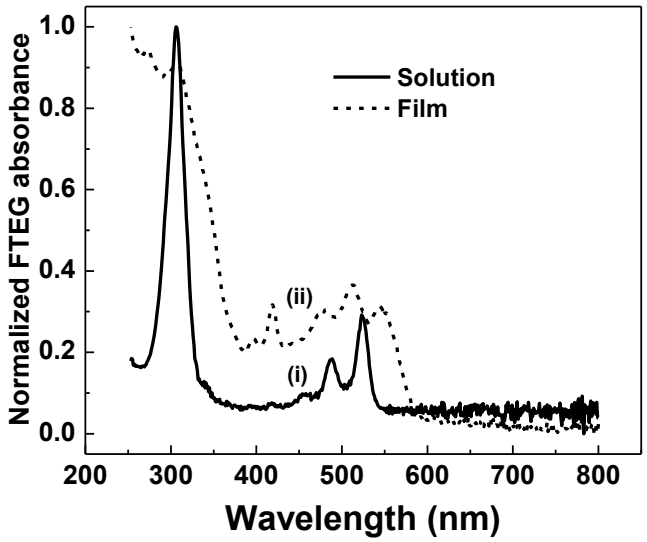

Figure 1.5 Absorption spectra of solution (i) and film (ii) of diF-TEG ADT

Two different effects typically occur in OPT channel layers as the result of

illumination: the photovoltaic and photoconductive effect. The photovoltaic effect occurs at the electrode/organic interface when the transistor operates in the on state ($|V_G| > |V_T|$, V_G more negative than V_T for a p-type device), whereas when V_G is more positive than V_T, the drain current increases proportionally to the optical power due to a photoconductive effect[11, 16]. As shown in Figure 1.6, the threshold voltage (V_T) shifts toward the positive direction (becoming easier to turn on) under illumination in both cases. For the PA-dielectric device, the shift of V_T was about 0.47 V and in the case of the SiO_2-dielectric device, ΔV_T was about 7.6 V. There have been several explanations of the shift of V_T under light illumination. Some believe the increasing of photo-induced carriers makes the Fermi level move closer to the edge of the highest occupied molecular orbital (HOMO). The degree of the energy level bending will decrease which leads to a shift of V_T toward the positive direction. Another explanation is that once the device is illuminated, there would be photo-induced electrons and holes. While the holes moved as part of the total current, the electrons were trapped in the positively charged trap states. Thus the V_T was positively shifted[17]. Wasapinyokul et al.[18] demonstrated that the apparent shift of the V_T of the device under illumination is entirely due to the photo-induced current and the intrinsic V_T remains constant both under illumination and in the dark.

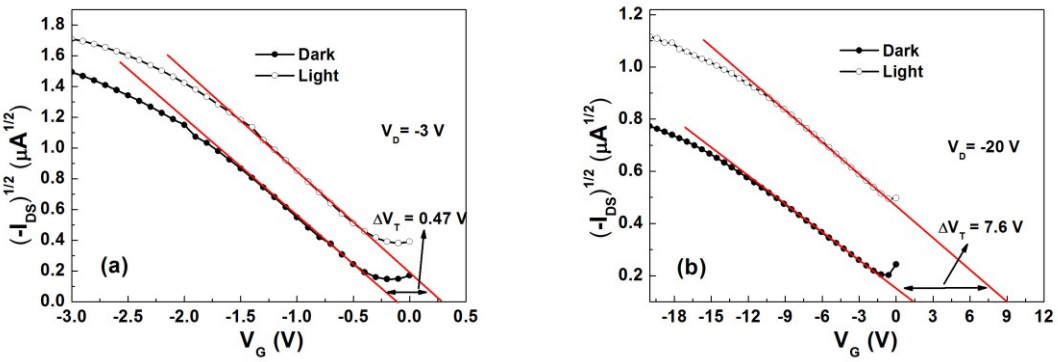

Figure 1.6 Shift in threshold voltage (V_T) for OPTs with (a) PA dielectric layer and (b) SiO_2 dielectric layer

1.3.2 Effect of different dielectric layers on OPT performance

When a gate voltage (V_G) is applied, the charge carriers will accumulate near the dielectric/organic interface. A conductive channel will be formed and the injected carriers from the source electrode will be transported through the channel. The conductive channel is located in just a few organic layers near the dielectric/organic interface. Therefore, the dielectric/organic interface influences both the performance and the functionality of OFETs. First, the trap density of the dielectric layer will affect the performance of the device. Second, the dielectric layer can be modified and this will change the surface energy which can influence the aggregation of the organic semiconductor. Third, the morphology of the organic semiconductor layer will be influenced by the roughness of the dielectric layer[19]. In addition, the thickness and capacitance of the dielectric layer can also affect the device performance dramatically[20]. In this project, we employed two kinds of dielectric layer: the

80-nm-thick potassium alumina (PA) layer and 300-nm-thick SiO_2 layer.

Figure 1.7 shows the increase of the drain current in the $I_D - V_D$ curves upon irradiation (365 nm-wavelength UV light, $P_{in} = 112\ \mu W/cm^2$) of OPTs with two kinds of dielectric layer. The devices were stored in the dark for 3 hours and then tested to ensure that the current was at a minimum. Then, the devices were illuminated and tested at 30 second intervals until the maximum current was reached. In the case of PA-dielectric device (Figure 1.7 (a) and (c)), the maximum increase between photocurrent and dark current was 1.45 μA ($V_D = -3\ V, V_G = -2.1\ V$) and the photoresponsivity (R) was $1.35\ A/W$, which was much larger than the performance of previous reported low-voltage OPTs ($> 1\ mA/W$)[13]. For the SiO_2-dielectric device, while the absolute current was lower, the ratio of the photocurrent to the dark current ($I_{DS,illu}/I_{DS,dark}$) reached 2.0×10^2 at $V_D = -20\ V$.

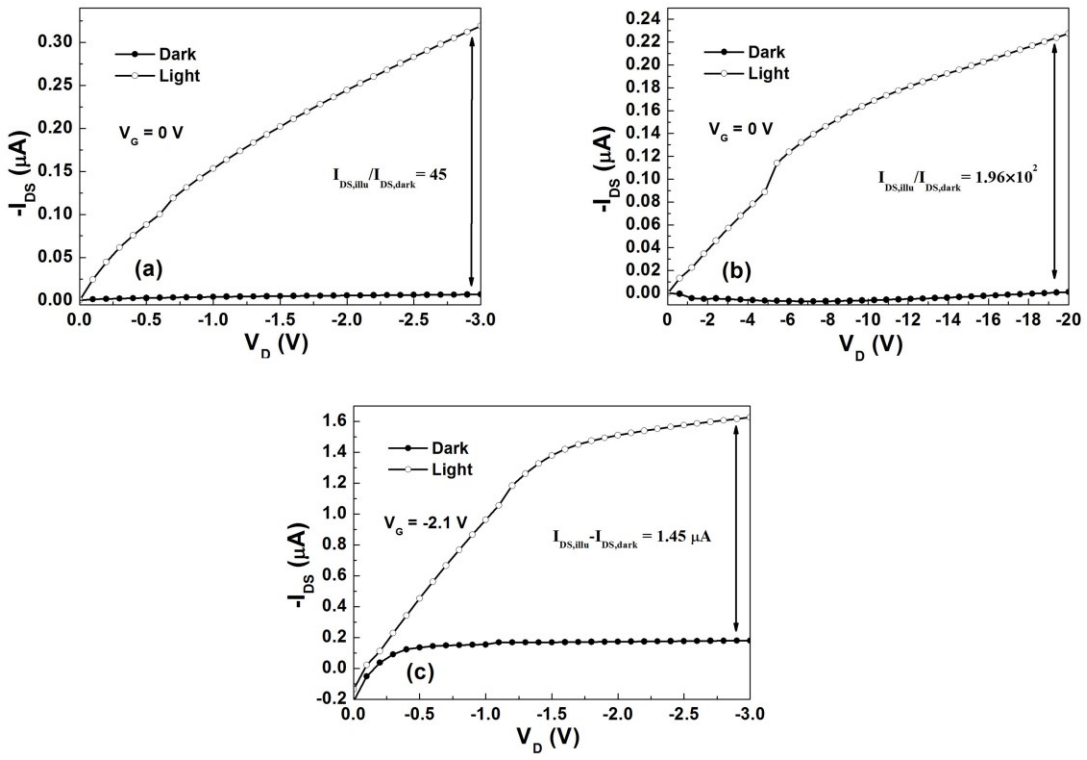

Figure 1.7 $I_D - V_D$ curves of OPTs at $V_G = 0\,V$ with (a) PA dielectric layer and (b) SiO_2 dielectric layer in the dark and under illumination. (c) $I_D - V_D$ curve of OPT with PA dielectric layer at $V_G = -2.1\,V$ in the dark and under illumination

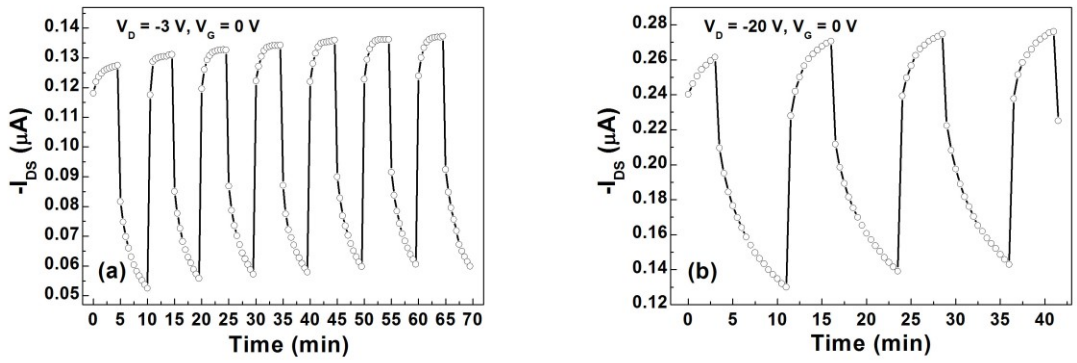

Figure 1.8 Photoswitching cycles of the OPTs with (a) PA dielectric layer and (b) SiO_2 dielectric layer illuminated by UV light ($V_G = 0\,V$)

More rapid photoswitching cycles are shown in Figure 1.8. The dynamic photocurrent was measured as a function of time at $V_D = -3\,V,\ V_G = 0\,V$ for a PA-dielectric device and $V_D = -20\,V,\ V_G = 0\,V$ for a SiO_2-dielectric device. As shown in Figure 1.8, due to the slow-relaxation processes involved in absorbing photons and detrapping localized electrons, the I_{DS} persists even after the illumination is removed[21] in both cases. The drain current increased immediately after the illumination, while decreased slowly after turning off the light. This observation demonstrated a different mechanism of photoresponse for this anthradithiophene device from the functionalized pentacene devices. For the primary mechanism of photo-induced conductivity in functionalized pentacenes, Tokumoto et al.[4] found that the photoresponse was temperature dependent and wavelength dependent. They believed that the light energy was absorbed, heating the sample locally in the region where the current density was greatest between the electrical contacts. Brooks et al.[10] reported the time and temperature dependent measurements of functionalized, single crystalline organic materials and demonstrated that carriers associated with the photo-excited states are thermally activated at low temperatures, with an energy less than both the intrinsic band-gap and the trap energy. For the diF-TEG ADT molecule, which exhibits intense solid-state fluorescence, the absorbed photons are not thermalized, they are re-emitted. The excited molecules under bias serve to provide more charge carriers; any that are not swept away will simply re-combine and emit. The slow-relaxation process also motivated the application of diF-TEG ADT-based device as photo-controlled memory. In addition, the plots clearly illustrated that the

switch-on current (I_{DS}) was very stable under ambient conditions. Moreover, it seems like I_{DS} gradually increased with cycling in both cases.

1.3.3 The performance of OPTs in high humidity

With appropriate electrical and optical properties, a key limitation for the application of an OPT is the stability in air and moisture. The stability of OPTs in air has been investigated by many groups[3, 22], especially the n-type OPTs[13, 23]. As far as moisture-stable organic phototransistors are concerned, very few studies have been published. As show in Figure 1.9 (a), I_{DS} was stable at high relative humidity (R.H.) up to 85%. However, with R.H. above 85%, a huge drop of I/I_o was observed. The photoswitching cycle of OPTs at 75% R.H is shown in Figure 1.9 (b) ($V_D = V_G = -20\ V$). SiO_2 was used as the dielectric layer and the wavelength of UV light was 365 nm. I_{DS} increased from 0.3 μA to 0.8 μA during 35 s irradiation. Unlike many other organic small molecule semiconmductors, diF-TEG ADT molecule is very stable in air and moisture.

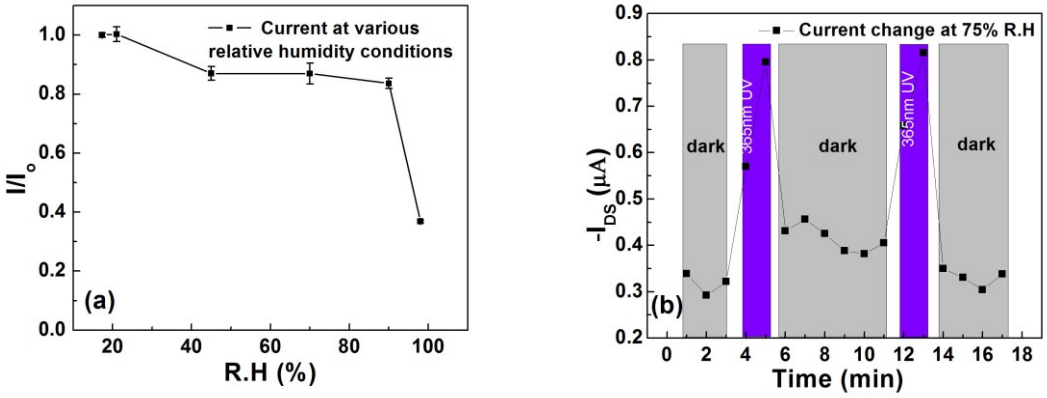

Figure 1.9 (a) I_{DS} at various relative humidities (R.H); (b) Photoswitching cycles of the OPTs illuminated by UV light at 75% R.H ($V_G = V_G = -20\ V$)

1.3.4 Effect of Connecting or disconnecting the gate electrode on OPT performance

An additional interesting observation is that the drain current (I_{DS}) changes significantly when connecting or disconnecting the grounded gate electrode to the device in the dark while V_D was -3 V. Figure 1.10 shows the photoswitching cycle of the device with multiple stable and reproducible states. Four stages can be obtained at $V_G = 0\ V$ via turning on/off light and connecting/disconnecting the gate electrode to the device: (1) light off + grounded gate ($V_G = 0\ V$), (2) light off + floating gate, (3) light on + grounded gate ($V_G = 0\ V$), (4) light on + floating gate. I_{DS} increased after removing the gate electrode when all other conditions were kept the same, as though the floating gate condition were somewhat "on". The photo-induced holes may have been accumulated at the dielectric/organic interface due to an effectively negative V_G. After reconnecting the gate probe to the device ($V_G = 0\ V$) after a light-on-light-off

cycle, the gate voltage was again fixed at 0 V. The photo-induced currents decreased rapidly when the light was turned off and the gate reconnected. Note that the photo-induced current cycle would have been that of Figure 1.8 (a) if the gate was not disconnected. Some previous literature reported that I_D could be adjusted by manipulating the negative gate voltage (V_G) during the light-off condition [5, 22], which was similar to what we found. This finding will encourage the application of diF-TEG ADT in multistage photo-controlled memory since it had multiple states under fixed illumination intensity, all seemingly without supplying any power to the gate.

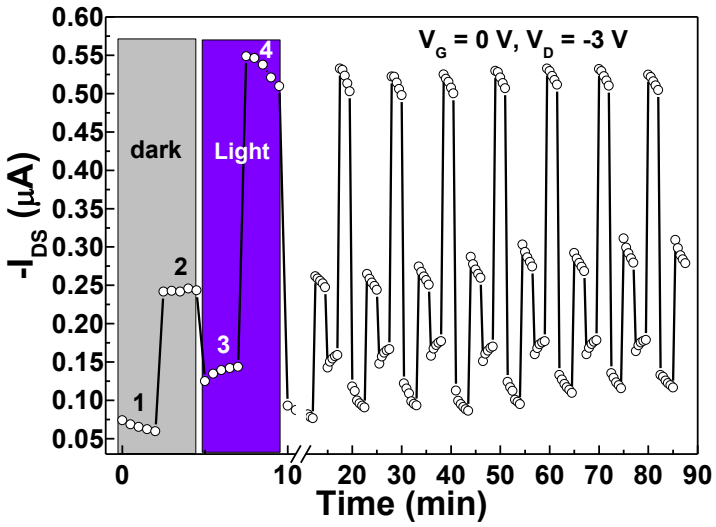

Figure 1.10 Drain current of photo-controlled memory operation at (1) light off + grounded gate (V_G = 0 V, V_D = -3 V), (2) light off + floating gate, (3) light on + grounded gate (V_G = 0 V, V_D = -3 V), (4) light on + floating gate

1.4 Conclusion

In summary, we demonstrated that highly soluble ADT-based material diF-TEG ADT can be used to fabricate low-voltage operated (-3 V) organic phototransistors. Thin film transistors were obtained using low-cost drop-casting process. Our results represent a step forward toward the possible use of these devices as battery-powered photosensors, for which it is preferred to achieve stable operation at lower voltages. The measured maximum photoresponsivity was $1.35\ \mathrm{A/W}$ at $112\ \mu\mathrm{W/cm^2}$ illumination intensity with PA dielectric layer, which is much higher than the performance of previous low-voltage OPT ($> 1\ \mathrm{mA/W}$)[13]. Meanwhile, the device with SiO_2 dielectric layer showed a photocurrent/dark-current ratio of 2.0×10^2. Performance in moist environments was promising; no sharp drop in drain current was observed until R.H reached 85%. Interestingly, a dramatic change in drain current was observed connecting or disconnecting the gate probe, motivating the possible application of diF-TEG ADT-based devices as a multistage photo-controlled memory.

Chapter 2

Biosensor Based on diF-TES ADT Molecular Solid

2.1 Introduction

Organic thin film transistors (OTFTs) based on solution-processed organic semiconductors have been investigated over the last decade for their potential application in sensor platforms because of their ability to make flexible and large-area electronics. Among the solution-processed organic semiconductors, small molecules have attracted much attention since they provide high field-effect mobility[1]. However, the morphology anisotropies lead to device-to-device variation and make it more difficult to print small molecule semiconductors on large substrates.

Polymer-small molecule blend organic transistors attracted much attention because polymers demonstrate excellent device uniformity[24]. Moreover, the solution rheology of polymers makes it possible to print organic semiconductors onto flexible substrates, which leads to a promising application for OFETs as low-cost, portable devices.

In this project, we blended small molecule diF-TES ADT (as show in Figure 2.1) with poly(methyl methacrylate) (PMMA). The phase-separated interface of diF-TES ADT and PMMA provided greater stability for the bottom gate - top contact transistor. A previous report demonstrated that the polymer-small molecule blend transistor

displayed higher field-effect mobility and greater stability than a homo diF-TES ADT film because the phase-separated interface provides an efficient pathway for charge transport[25].

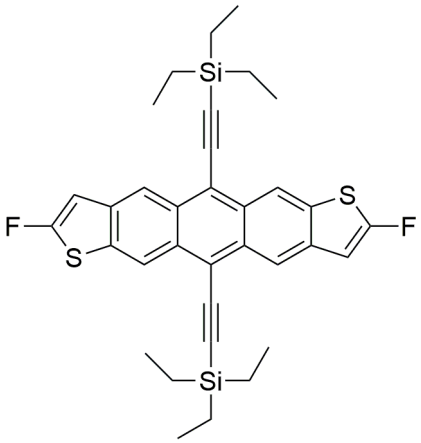

Figure 2.1 The molecular structure of diF-TES ADT

We investigated the transistor response to antibody using anti-bovine serum albumin (BSA) as the target antibody since BSA shares many similarities with human serum albumin (HSA) in bio-function and bio-chemical properties, making it a good model for a clinical interferent[26]. Both BSA and rabbit anti-BSA are negatively charged when immersed in solution (pH 7.4)[27].

2.2 Experimental Section

2.2.1 Materials and device fabrication

The diF-TES ADT was synthesized as previously reported by Anthony[28]. The OTFTs

were fabricated with a bottom-gate, top-contact configuration. A heavily doped n-type Si wafer was used as the gate electrode. The wafer was cleaned with ultrasonication in piranha solution **(DANGER! Highly corrosive to skin!)**, acetone and isopropanol, and dried by forced nitrogen gas. 70-nm-thick thermally grown SiO_2 was used as the dielectric layer. The semiconductor thin film was prepared by first spin-coating diF-TES ADT/PMMA (1:1 w/w) blend solution (20 mg/mL) in chlorobenzene onto the dielectric layer at a speed of 1500 rpm for 60 seconds, followed by moving the sample into a vacuum oven at room temperature and leaving it overnight to remove the residual solvent. Then the gold source and drain electrodes (50 nm) were thermally evaporated through an interdigitated mask (as shown in Figure 2.2, channel width/length (77 000μm/250μm)) at 0.3 $\dot{A}\,s^{-1}$. The deposition chamber pressure was $<5\times10^{-6}$ Torr.

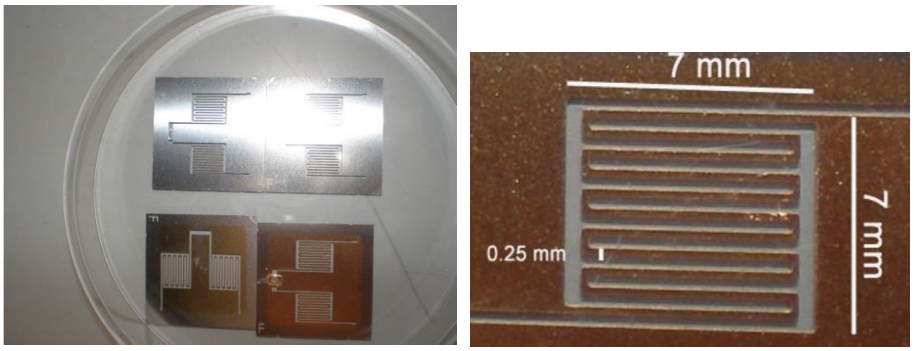

Figure 2.2 The interdigitated electrode mask used for fabricating devices (the distance between two neighboring electrodes is 0.25 mm, indicated as short white line)[26]

The structure of the biosensor based on the diF-TES ADT/PMMA blend transistor is

shown in Figure 2.3. 25 nm tetratetracontane (C44) was then thermally evaporated on Au electrodes to protect electrodes against any trace amount of buffer solution that may penetrate through the CYTOP layer. CYTOP (9% weight, Bellex International Corporation) was spin-coated on the device surface (6000 rpm, 90 s) and another layer of C44 (50 nm) was thermally evaporated onto the CYTOP layer to fill any residual pinholes in the CYTOP layer. Then an N-hydroxysuccinimide (NHS) treated PS-*block*-PAA ((poly(styrene)-*block*-poly(acrylic acid)) layer was spin-coated on the C44 layer at a speed of 3000 rpm for 90 seconds. The carboxylic acid groups of PS-*block*-PAA were activated as previous work demonstrated[26]. Finally, the device was dipped into DI water several times to remove excess NHS and other residuals, and dried with nitrogen flow.

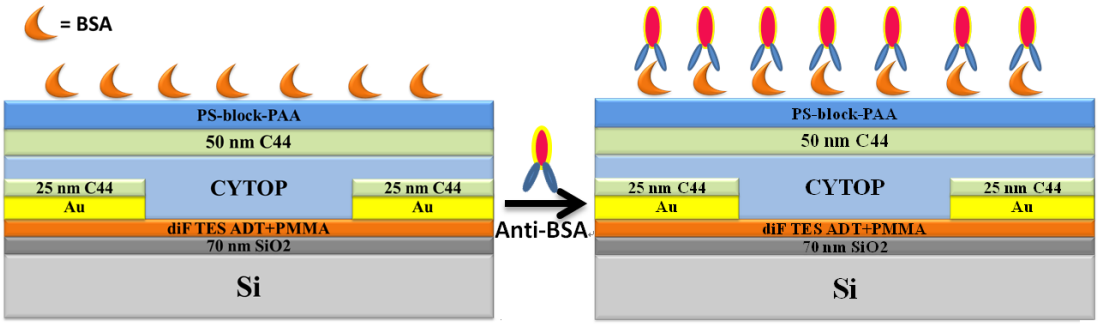

Figure 2.3 Device architecture of biosensor based on diF-TES ADT/PMMA blend transistor

BSA was covalently attached to the activated PS-*block*- PAA surface from a 10 mg/mL BSA solution for more than 8 hours at room temperature, and then gently rinsed with DI water to remove any non-covalently bound materials.

For the device which was used as a pH sensor, the thermally evaporated C44 (50 nm)

layer was the last step and no PS-*block*-PAA layer was used.

2.2.2 Electrical and anti-BSA response characterization of the devices

All the OTFTs were characterized using an Agilent 4155C semiconductor analyzer. During the characterization of responses to pH, $V_D = -2\,V$ was used, while $V_D = -3\,V$ was fixed when measuring responses to anti-BSA. Various concentrations of anti-BSA solution were introduced onto devices as $100\,\mu L$ via micropipette. In order to prevent water evaporation, the measurements were conducted in a water-vapor-saturated environment.

2.3 Results and Discussion

2.3.1 pH sensor based on diF-TES ADT: PMMA blend transistor

Figure 2.4 shows the transfer curve (a) and output curve (b) of the small molecule-polymer blend organic transistor. As shown in the figure, the drain current reached 140 nA at V_G = -2 V ($V_D = -2\,V$).

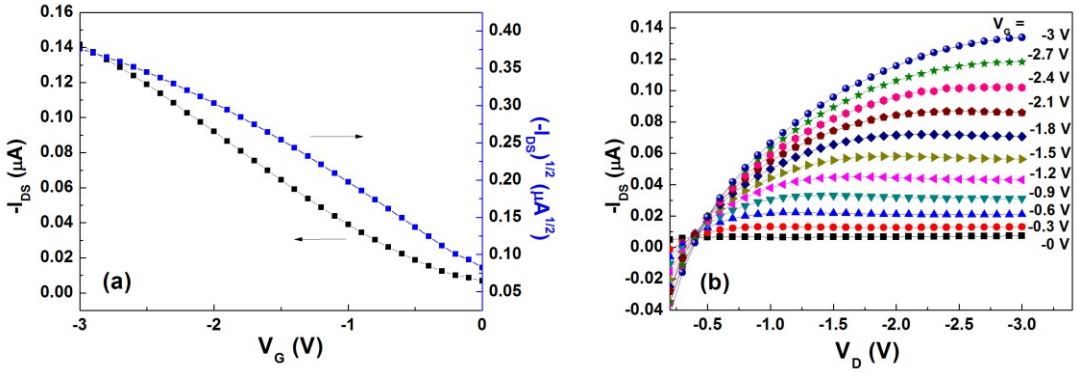

Figure 2.4 The transfer (a) and output (b) curves of diF-TES ADT/PMMA blend TFT

As shown in Figure 2.5, the pH sensor performances of the polymer-small molecule blend TFT devices were determined by measuring drain current changes on exposure to varying pH solution. Two couples of pH solutions were used: pH 4 & pH 10 and pH 2 & pH 12. The drain currents at $V_G = -2\,V$ in both acid and base solutions were used to compare the response to different pH. The change of drain current was 9.2 % for the pH 4 & pH 10 couple (Figure 2.5 (a)), while it was 6.4 % for the pH 2 & pH 12 couple (Figure 2.5 (a)). At lower voltages, the current changes were more similar.

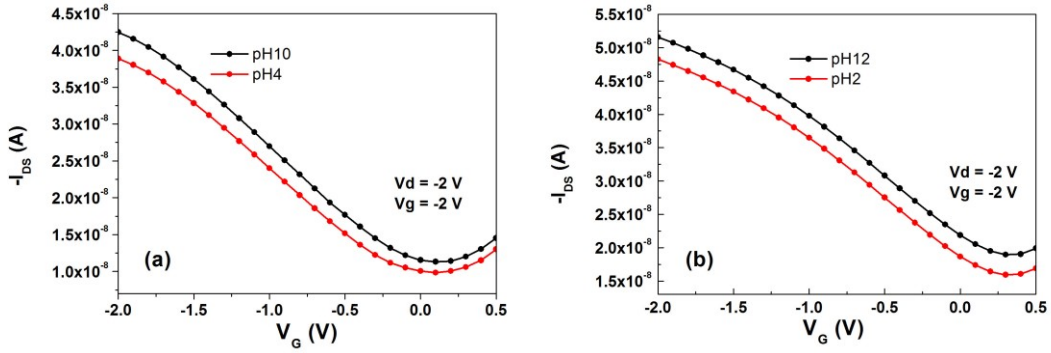

Figure 2.5 The I_D-V_G curves of pH sensor based on diF-TES ADT/PMMA blend TFT

Moreover, the stability of the small molecule-polymer blend TFT in air improved significantly compared to the homo diF-TES ADT film. As shown in Figure 2.6, the mobility of the TFT device increased in the first 10 days because of the O_2 doping. Then the mobility decreased because of the degradation of diF-TES ADT in air. However, the homo diF-TES ADT thin film transistor cannot operate after storage for more than two weeks in air.

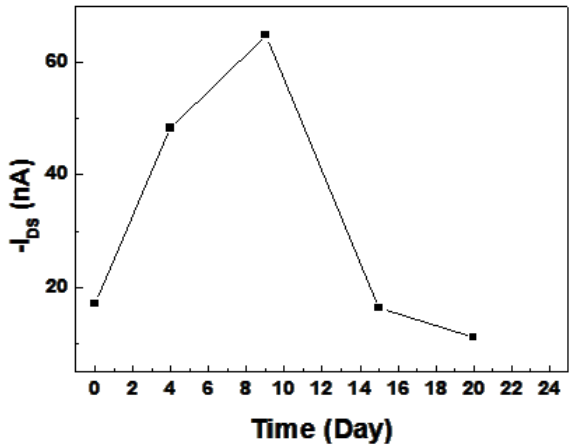

Figure 2.6 The stability of diF-TES ADT/PMMA blend TFT in air

2.3.2 Biosensor based on diF-TES ADT: PMMA blend transistor

Figure 2.7 shows the current changes of a BSA-coated transistor by switching between 0.05 PBS and anti-BSA solutions. When switching between 0.05 PBS solutions, the drain current always drifted to the higher value. Drain current increased due to ion or $H3O^+$ doping. After adding anti-BSA solution on the device, the drifting of drain current slowed down (Figure 2.7). To make it more clear, a simple linear regression was used to fit a straight line (red line in the figure, the equation was

shown in equation 2.1) through the set of these points and made the sum of squared residuals as small as possible.

$$y = -4.422 \times 10^{-10}\, x - 2.878 \times 10^{-7} \qquad (2.1)$$

After calibrating (compensate the effect of ion doping), the drain current actually decreased in the presence of anti-BSA. The drain current drifting direction in anti-BSA solution was opposite to that in pure 0.05 PBS solution, as shown in Figure 2.8. The drain current change demonstrated that attaching negatively charged species induces lower conductance in p-channel transistors. One possible mechanism is that negatively charged BSA pulls charge carriers (holes) away from the channel region for a p type transistor as suggested in previous literature[26, 29]. Another explanation is that the anti-BSA binding rearranges dipole moments to create a local field that decreases the hole density of the semiconductor. Distinguishing between such mechanisms is the subject of ongoing research.

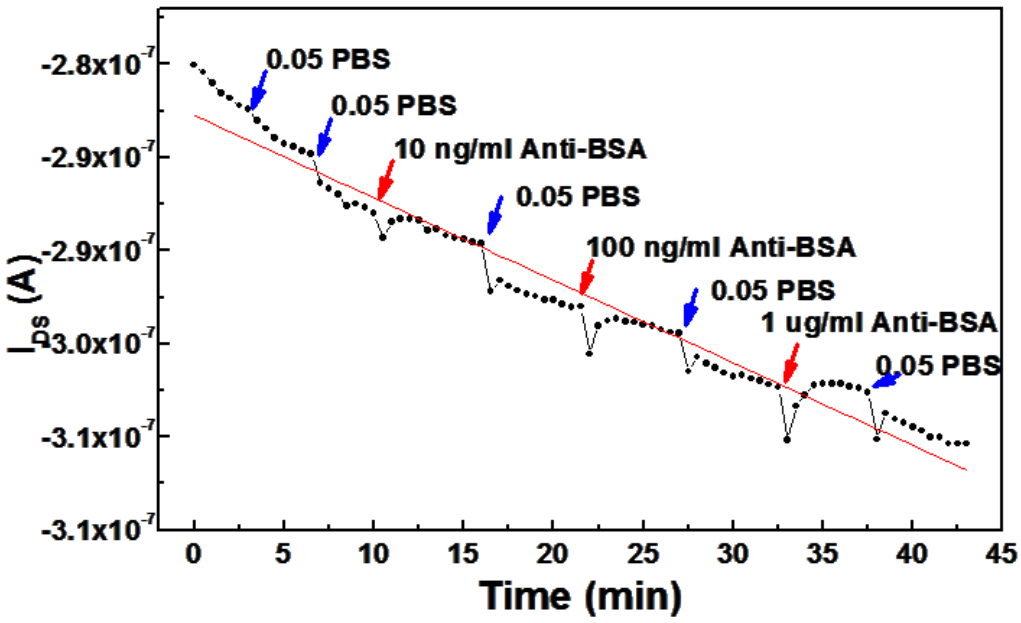

Figure 2.7 Current changes by switching between 0.05pbs and anti-BSA 0.05pbs solutions with linear fitting line

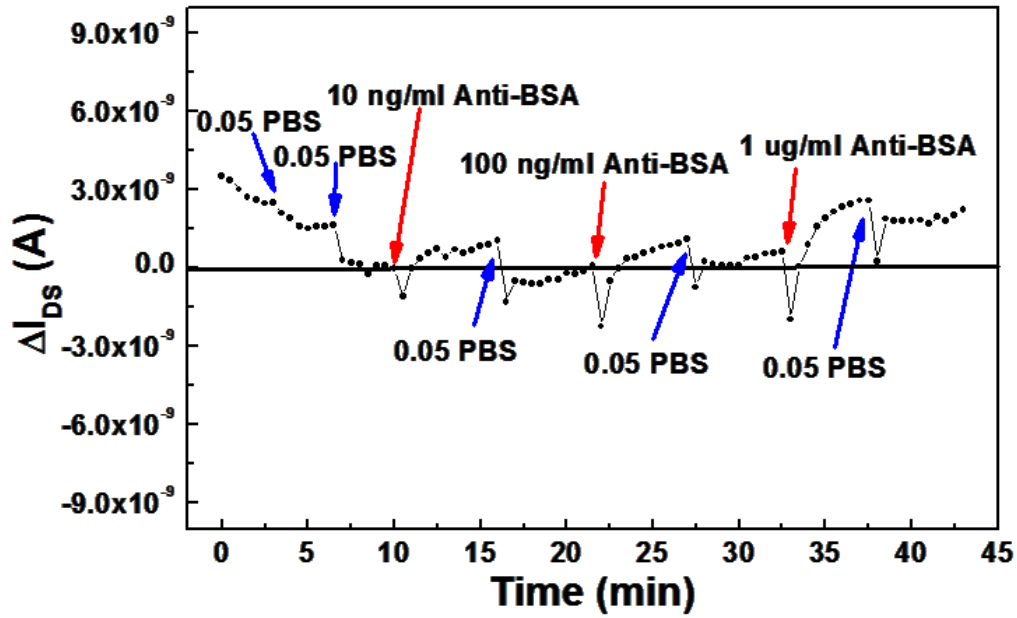

Figure 2.8 Extracted data after calibrating by linear fitting line

The “0 value” of ΔI_{DS} was set to be the current when adding the addition of anti-BSA (10ng/mL anti BSA) was begun, and a “0 value line” across Figure 2.8 is the horizontal projection of this point. The dots above “0 value line” represent drain current decrease, while the dots below this line represent drain current increase. As shown in Figure 2.8, after exposure to anti-BSA solution, drain current always decreases. Moreover, after each exposure cycle to anti-BSA, rinsing the surface with 0.05 PBS cannot bring the current value back to the “0 value line” completely, indicating irreversible and specific binding between BSA and anti-BSA on the device surface.

There are several reasons for the lower response (several nA) of this biosensor than our previous system[26]. First, 50 nm C44 instead of 16 nm C44 was applied to increase device stability in 0.05 PBS solution. Thicker C44 led to a longer distance for the capacitive coupling to holes in the vertical direction. Secondly, the anti-BSA size is large, which may lead to some part of bonded anti-BSA molecules located outside of the electrical double layer above the device. Further device optimization is possible.

2.4 Conclusion

The polymer-small molecule blend thin film transistor has a promising application in the sensor field. We have developed a sensitive (10 ng/mL) sensor platform for anti-bovine serum albumin (anti-BSA) detection using small molecule-polymer blend

transistors. The advantages of this particular material combination include printability, higher stability in 0.05 PBS solution and less leakage current caused by ion doping. The change of drain current for the pH 4 & pH 10 couple, and for the pH 2 & pH 12 couple are similar up to $V_g = -2\,V$. Although the response to anti-BSA was smaller than the response to pH, the drain current displays a change even at the switching of 0.05 PBS solution and 10 ng/mL anti-BSA solution.

Chapter 3

Conclusions and Perspectives

3.1 Conclusions

This thesis discusses the application of solution-processed low-voltage organic field-effect transistors based on anthradithiophene molecular solids, including organic phototransistors (OPTs) that response to UV light, and sensors that response to pH and antibody.

We demonstrated that highly soluble ADT-based material diF-TEG ADT can be used to fabricate low-voltage operated (-3 V) organic phototransistors. The results represent a step forward toward the possible use of these devices as battery-powered photosensors, for which it is preferred to achieve stable operation at lower voltages. The measured maximum photoresponsivity was $1.35\ \mathrm{A/W}$ at $112\ \mu\mathrm{W/cm^2}$ illumination intensity with PA dielectric layer. Performance in moist environment was

promising; no sharp drop in drain current was observed until R.H reached 85%. A dramatic change in drain current was observed connecting or disconnecting the gate probe, which motivates the possible application of diF-TEG ADT-based devices as a multistage photo-controlled memory.

Another promising application for the ADT-based material is the thin film transistor (TFT). We have developed a sensitive (10 ng/mL) sensor platform for bovine serum albumin (BSA) detection using small molecule-polymer blend transistors. Blending PMMA with diF-TES ADT improved the environmental and electrical stability because of its reported vertically phase-separated structure. Moreover, after blending with polymer, diF-TES ADT became easier to print on large flexible substrates.

3.2 Future perspectives

In the study of organic phototransistors, the mechanism for the current change when connecting or disconnecting the gate probe is still uncertain. More research needs to be done to obtain a convincing explanation for this phenomenon. Also, the large leakage current was the primary cause of the low photocurrent/dark-current ratio. In future works, the dielectric layer should be modified to decrease the leakage current. A solution-processed, low-temperature annealed dielectric layer can be applied in this system to develop low-cost, large-area flexible organic phototransistors.

Sensors with higher sensitivity and faster response speed are highly desired in the

medical device field. Several strategies can be employed to improve the performance of small molecule-polymer blend TFT sensor. First, the thickness of C44 layer deposited on the CYTOP layer can be adjust to ensure the stability as well as get higher sensitivity. Second, different kinds of dielectric layers should be tried to get higher drain current. Last, an extended-gate top-contact structure can be used to simplify the structure of the sensor. The covalent attachment of anti-BSA to the BSA can be formed on the surface of the extended gate, which means no C44 and CYTOP layer are needed on the organic semiconductor layer.

Bibliography

[1] Y. Mei, M. Loth, M. Payne, W. Zhang, J. Smith, C. Day, S. Parkin, M. Heeney, I. McCulloch, T. Anthopoulos, J. Anthony, O. Jurchescu, Advanced materials (Deerfield Beach, Fla.) 2013, 25, 4352.

[2] L. Ruipeng, K. Hadayat Ullah, M. P. Marcia, M. S. Detlef, E. A. John, A. Aram, Advanced Functional Materials 2013, 23; D. J. Oana, S. Sankar, R. J. Kline, D. H. Steven, E. A. John, N. J. Thomas, J. G. David, Chemistry of Materials 2008, 20.

[3] G. Yunlong, D. Chunyan, D. Chong-an, Z. Jian, S. Xiangnan, W. Yugeng, Z. Lei, W. Weiping, Y. Gui, L. Yunqi, Applied Physics Letters 2009, 94.

[4] T. Tokumoto, J. S. Brooks, R. Clinite, X. Wei, J. E. Anthony, D. L. Eaton, S. R. Parkin, Journal of Applied Physics 2002, 92.

[5] K. Kim, S. Bae, Y. Kim, J. Hur, M. Hoang, T. Lee, M. Cho, Y. Kim, M. Kim, J.-I. Jin, S.-J. Kim, K. Lee, S. Lee, D. Choi, Advanced materials (Deerfield Beach, Fla.) 2011, 23, 3095.

[6] Y. Kim, S. Bae, K. Kim, T. Lee, J. Hur, M. Hoang, M. Cho, S.-J. Kim, Y. Kim, M. Kim, K. Lee, S. Lee, D. Choi, Chemical communications (Cambridge, England) 2011, 47, 8907.

[7] G. Yunlong, D. Chunyan, Y. Gui, D. Chong-an, J. Shidong, X. Hongxia, Z. Jian, Y. Shouke, Y. Cailan, H. Wenping, L. Yunqi, Advanced Functional Materials 2010, 20.

[8] M. El Gemayel, M. Treier, C. Musumeci, C. Li, K. Müllen, P. Samorì,

Journal of the American Chemical Society 2012, 134, 2429.

[9] W. Nicola, C. Andrea, B. Daniele, K. Jaroslav, J. Jan, D. Daniel, M. Gaudenzio, IEEE Transactions on Nuclear Science 2011, 58.

[10] J. S. Brooks, T. Tokumoto, E. S. Choi, D. Graf, N. Biskup, D. L. Eaton, J. E. Anthony, S. A. Odom, Journal of Applied Physics 2004, 96.

[11] L. Bruno, T. Thierry, V.-A. Christine, Polymer International 2012, 61.

[12] J. G. Labram, P. H. Wöbkenberg, D. D. C. Bradley, T. D. Anthopoulos, Organic Electronics 2010, 11.

[13] M. Biswanath, M. Moumita, S. Kyoseung, P. Seungmoon, Journal of Materials Chemistry 2011, 21.

[14] L. Yu, G. Pengfei, Z. Bo, L. F. Michael, E. K. Howard, Chemistry of Materials 2013, 25.

[15] W. Xuhua, W. Kamol, T. Wei De, R. Ruth, J. C. Alasdair, D. C. B. Donal, Journal of Applied Physics 2010, 107.

[16] K.-J. Baeg, M. Binda, D. Natali, M. Caironi, Y.-Y. Noh, Advanced materials (Deerfield Beach, Fla.) 2013, 25, 4267.

[17] Y. Feng, L. Jinhua, M. Sheung Man, Journal of Applied Physics 2009, 106.

[18] W. Kamol, W. I. Milne, D. P. Chu, Journal of Applied Physics 2011, 109.

[19] C.-a. Di, Y. Liu, G. Yu, D. Zhu, Accounts of chemical research 2009, 42, 1573.

[20] C.-a. Di, F. Zhang, D. Zhu, Advanced materials (Deerfield Beach, Fla.) 2013, 25, 313.

[21] M. Barra, F. Bloisi, A. Cassinese, F. V. D. Girolamo, L. Vicari, Journal of Applied Physics 2009, 106.

[22] M. Hoang, Y. Kim, M. Kim, K. Kim, T. Lee, D. Nguyen, S.-J. Kim, K. Lee, S. Lee, D. Choi, Advanced materials (Deerfield Beach, Fla.) 2012, 24, 5363.

[23] Y. Che, X. Yang, G. Liu, C. Yu, H. Ji, J. Zuo, J. Zhao, L. Zang, Journal of the American Chemical Society 2010, 132, 5743.

[24] H. Richard, S. Jeremy, O. Simon, H. Martin, E. A. John, M. Iain, V. Janos, D. C. B. Donal, D. A. Thomas, Advanced Materials 2009, 21.

[25] L. Wi Hyoung, K. Donghoon, E. A. John, L. Hwa Sung, C. Hyun Ho, K. Do Hwan, L. Seung Goo, C. Kilwon, Advanced Functional Materials 2012, 22.

[26] H. Weiguo, B. Kalpana, L. Rachel, D. Pratima, S. Jasmine, F. M. H. Josue, P. Christian, S. Julia, D. E. Allen, F. Joelle, B. Michael, E. K. Howard, Chemical Science 2014, 5.

[27] C. Wang, J. Wang, L. Deng, Nanoscale research letters 2011, 6, 579.

[28] S. Subramanian, S. Park, S. Parkin, V. Podzorov, T. Jackson, J. Anthony, Journal of the American Chemical Society 2008, 130, 2706.

[29] H. Khan, J. Jang, J.-J. Kim, W. Knoll, Journal of the American Chemical Society 2011, 133, 2170.

Curriculum Vita

Wenmin Guo was born on April 18, 1988 in Fenyang, Shanxi Province, China. She received her Bachelor's Degree at China University of Geosciences, Beijing majoring in Materials Chemistry in 2011. She had an one year internship at Chinese Academy of Sciences and completed her graduate project there. She joined the Materials Science and Engineering Department at Johns Hopkins University in 2012, started to work in Professor Howard Katz's group. Her research involved developing the organic field-effect transistors (OFETs) for photosensor application and fabricating antibody-based biosensor. Important publications to date include:

- Wenmin Guo, Yu Liu, Weiguo Huang, Marcia M. Payne, John Anthony, and Howard E. Katz. Solution-processed Low-voltage Organic Phototransistors Based on an Anthradithiophene Molecular Solid. *Organic Electronics. Under review*
- Wenmin Guo, Yihe Zhang, Wei Zhang. Mechanical properties and crystallization behavior of hydroxyapatite/poly(butylenes succinate) composites. *Journal of Biomedical Materials Research Part A*. 2013, 101A, 9, 2500-2506.
- Wenmin Guo, Yihe Zhang, Baolin Cui. The preparation and characterization of red mud based porous materials with pore-forming agents. *5th International Conference on Bioinformatics and Biomedical Engineering, iCBBE 2011*. DOI:10.1109/icbbe.2011.5781454.
- Yihe Zhang, Bo Lu, Fengzhu Lv, Wenmin Guo, Junhui Ji, Paul K. Chu, Changan Zhang. Effect of processing conditions on poly(butylene succinate) foam materials. *Journal of Applied Polymer Science*. 2012, 126, 2, 756-761.

- Yihe Zhang, Wei Chen, Guocheng Lv, Fengzhu, Lv, Paul K. Chu, Wenmin Guo, Baolin Cui, Rui Zhang, Heli Wang. Adsorption of polyvinyl alcohol from wastewater by sintered porous red mud. *Water Science & Technology*. 2012, 65, 11, 2055-2060.
- Li Yu, Yihe Zhang, Wangshu Tong, Jiwu Shang, Fengzhu Lv, Paul K. Chu, Wenmin Guo. Hierarchical composites of conductivity controllable polyaniline layers on the exfoliated graphite for dielectric application. *Composites Part A*. 2012, 43, 11, 2039-2045.
- Srinivas Kola, Joo Kim, Robert Ireland, Mingling Yeh, Kelly Smith, Wenmin Guo, Howard Katz. Pyromellitic diimide – ethynylene based homopolymer film as an n-channel organic field-effect transistor semiconductor. *ACS Macro Letters*. 2013, 2, 8, 664–669.